Published as:

Reches, Z., 1998, Tensile fracturing of stiff rock layers under triaxial compressive stress states, 3rd NARMS, Mexcio, June, 1998, Int. J. of Rock Mech. & Min. Sci. 35: 4-5, Paper No. 70

Tensile Fracturing of Stiff Rock Layers Under Triaxial Compressive Stress States

Ze'ev Reches

Institute of Earth Sciences, Hebrew University, Jerusalem 91904, Israel; reches@earth.es.huji.ac.il

ABSTRACT

We studied the fracturing processes of stiff limestone layers embedded in compliant silty and sandy layers of Carmel Formation, Cedar Mountain area, central Utah. The studied limestone layers are intensely fractured by two or three sets of tensile fractures and small faults. Fracture density is anomalously high: up to 165 fractures/meter in a 0.065 m thick layer. The intense fracturing is interpreted here as reflecting stress amplification inside the limestone layers. Eshelby's inclusion analysis is used to show that regional compressive stresses, which are associated with overburden and tectonic loading, could generate tensile stresses of high magnitude within the limestone layers.

KEYWORDS

rock mechanics, fracture, tension, joints, inclusion, Eshelby's model, layers, stress amplification, strength

INTRODUCTION

Sequences of sedimentary rocks are composed of layers with different mechanical properties that are juxtaposed one above the other. These sequences include alternations of brittle and ductile layers and alternations of stiff and compliant layers. In brittle/ductile sequences, the brittle layers tend to yield by tensile jointing or by shear fracturing, while the ductile layers tend to flow with no or little apparent fracturing. One can envision that the contrasts of brittleness and stiffness between layers is a dominant factor in controlling the development of joints and small faults in sedimentary rocks. We present here a quantitative model to analyze this effect on fracturing of sedimentary layers.

Many field observations demonstrated the influence of layering on jointing. Hodgson (1961) showed that many joints tend to terminate at bedding contacts. Harris et al. (1960) and Murray (1968) showed that joint spacing can be correlated with the thickness of layers, the relative competence of the layers, and the intensity of local structural deformation; and, in general, thin, brittle layers in highly deformed zones are intensely jointed. These properties of joint sets may strongly affect the quality of a fractured reservoir (e.g., Nelson, 1985), and its geotechnical properties. Another observation is that fractures may be restricted to the more brittle layers, terminating toward unfractured, more ductile layers (Lorenz et al., 1991). For example, the highly siliceous, brittle layers in Monterey Formation, California, are intensively jointed by closely spaced fractures, whereas the alternating, more shaley layers are jointed by large and widely spaced fractures.

FIELD OBSERVATIONS

We present some features of tensile fractures in Carmel Formation, Cedar Mountain area, central Utah. The lower Carmel Formation

exposed in this region includes thin-layered sequence of shaley siltstones, fine grain sandstones, mudstone, limestones and gypsum layers (Krantz, 1986). The current work concentrates on four to eight prominent limestone layers of this unit. These layers range in thickness from 5 cm to 75 cm, and their horizontal extent is up to a few hundreds meter (Figure 1). The limestone is hard, dark-gray in color and fine to medium in grain size, and limestone layers form small cliffs within the much softer layers of the shaley siltstones (Figure 1).

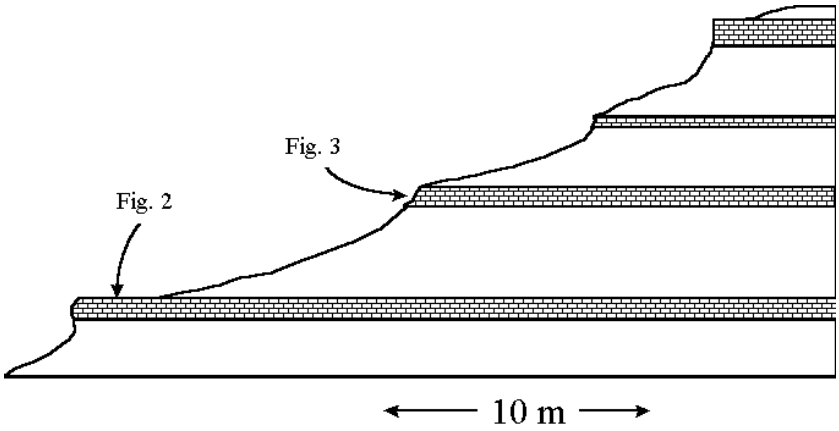

Figure 1: Schematic section of part of the Carmel Formation in Cedar Mountain area. Gray zones- indicate limestone layers; blank regions-silty/shaley layers.

The limestone layers in Cedar Mountain area are intensely fractured by two or three sets of tensile fractures. These fractures are noticeably smooth and planar with faint plumose structures. Fractures of one set usually cross-cut fractures of other sets without curving. Figure 2 is a map of a characteristic exposure showing the fracture traces observed on top of 0.5 m thick limestone layer. The map and its rose diagram show two dominant sets, one trending 74° ± 12° and the second trending 117° ± 19° . Most of the fractures are normal to the bedding surfaces, and many cross the layers from top to base (Figure 3).

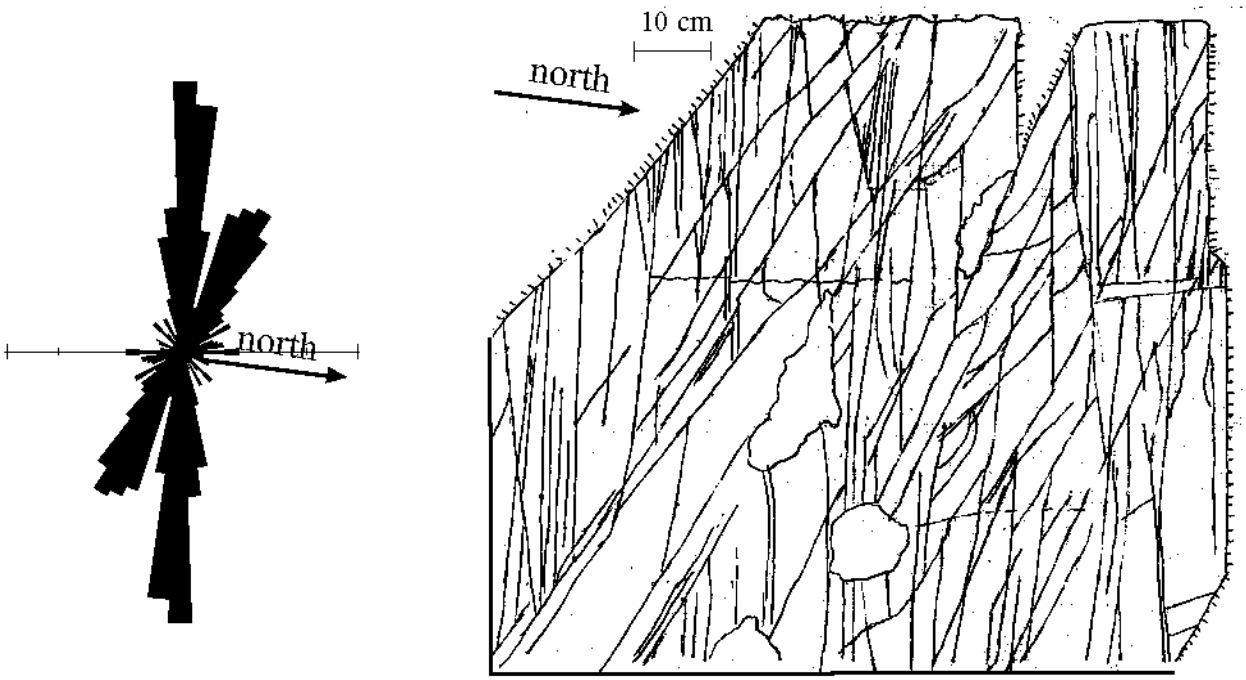

Figure 2: Fracture trace map on top of a limestone layer (right), and rose diagram of fracture orientations calculated by segment length (left). Total fracture trace length is 45 m. Location in Figure 1.

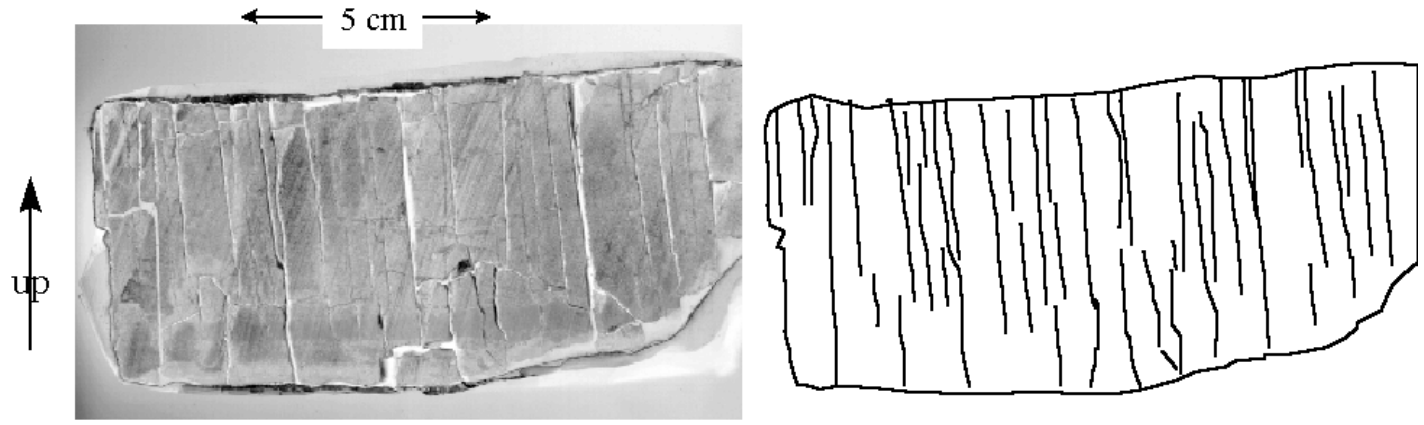

a.

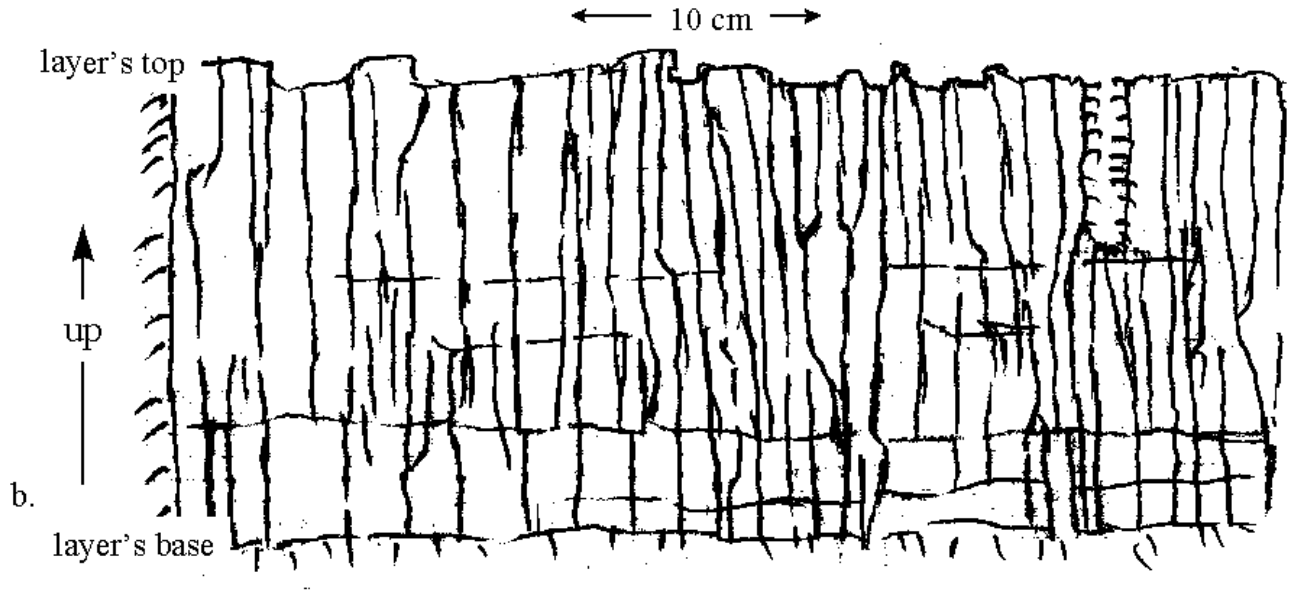

Figure 3: Side views of fracture patterns in two limestone layers (view position marked in Figure 1).

a. Left- photograph; right-line drawing. B. Field map of fracture traces.

Probably the most striking feature of the studied tensile fractures is the anomalously high fracture density. Fracture density is the number of fractures counted along a line normal to the fractures, and usually it is represented by its inverse, mean spacing between fractures. Fracture density depends on several parameters including mechanical properties, intensity of strain and stress and thickness of the fractured layers (e.g., Price and Corsgrove, 1990). In gently deformed regions, like the study area, fracture spacing is approximately equal to layer thickness (lines A and B in Figure 4). The present limestone layers display different relations. Figure 3a displays mean fracture spacing of ≈ 0.006 m (or density of ≈ 165 fractures/meter) in a 0.065 m thick layer. Figure 3b shows mean fracture spacing of ≈ 0.0125 m (or density of ≈ 80 fractures/meter) in a 0.18 m thick layer. Fractures density can also be estimated from the cumulative length of the fracture traces in map view. In Figure 2, there are ≈ 45 m of fracture traces per square meter in a layer of 0.5 m thick. This corresponds to mean spacing of ≈ 0.022 m (or density of ≈ 45 fractures/meter) in a 0.5 m thick layer.

The above spacing values appear as a distinct group with respect to published results (Figure 4). As these spacing values are not uncommon in Cedar Mountain area, we discuss below a possible explanation for their occurrence.

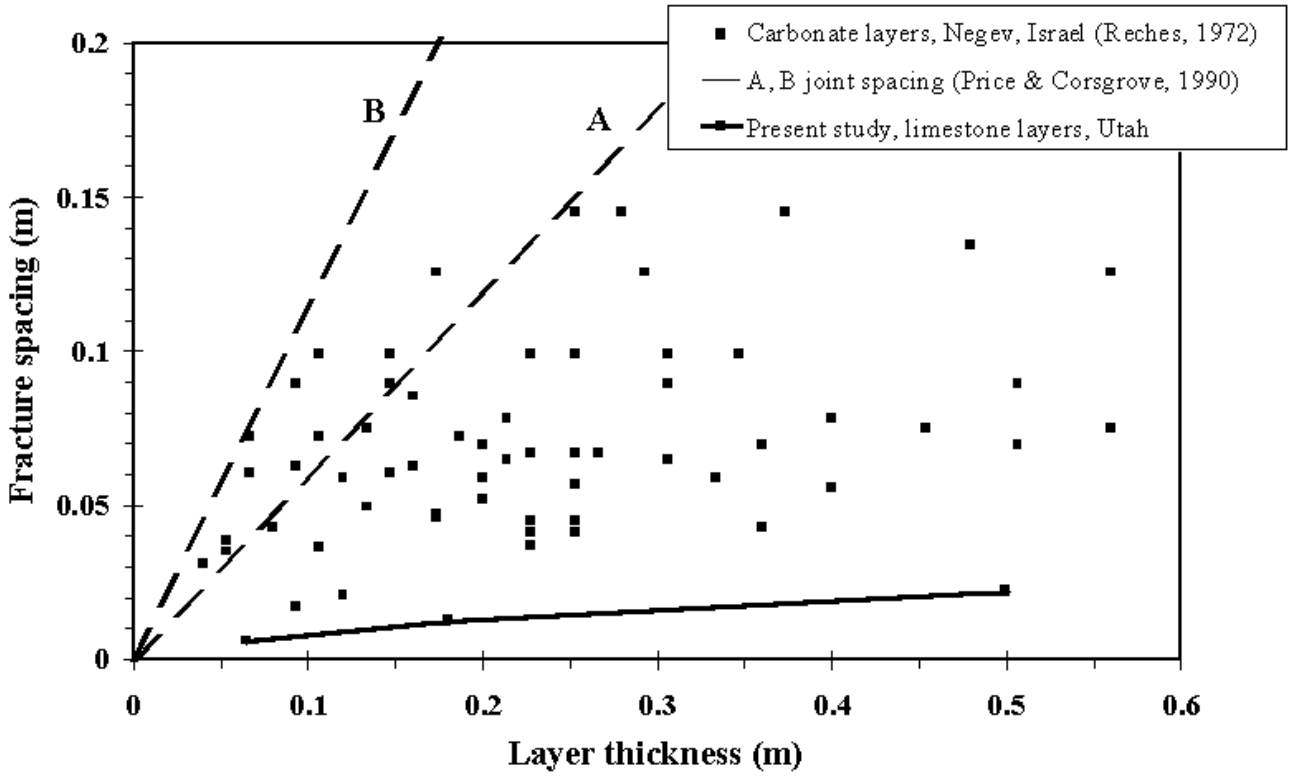

Figure 4: Fracture spacing as function of layer thickness in slightly deformed regions.

THEORETICAL ANALYSIS

Eshelby's Model

The high fracturing intensities observed in the limestone layers of Carmel Formation (Figures 1-4) suggest that stresses were amplified within these layers. We adopt here the approach of Eidelman and Reches (1992) who analyzed the tensile fracturing of stiff pebbles embedded in poorly consolidated conglomerates. As the host conglomerates could not transmit tensile stresses, these authors proposed that the tensile fracturing occurred due to the stress amplification associated with the stiffness contrast between the pebbles and the conglomerate. Eidelman and Reches (1992) presented a 2D solution (Figure 5) that was later expanded to 3D solution based on the inclusion model of Eshelby (Reches et. al, 1994; Eidelman, 1995). This solution is further developed here.

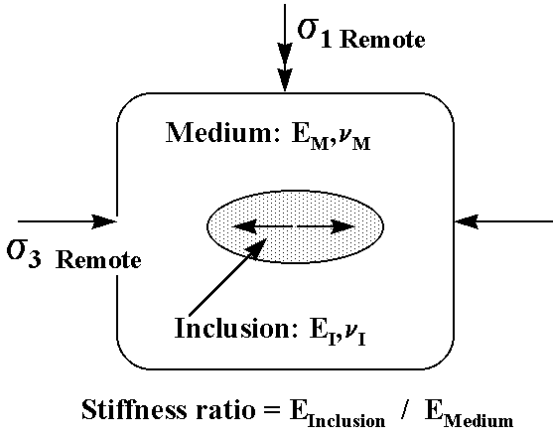

Figure 5: A 2D presentation of the inclusion model

Eshelby (1957) calculated the stress states in a stiff ellipsoidal inclusion embedded in soft medium. Eshelby's derivations were used in many later analyses of composite material (e.g., Mura, 1987; Zhao and Weng, 1990), seismic waves in rocks, and the strength of

fault zones. We use here the approach of Mura (1987), Benveniste (1987) and Zhao and Weng (1990) who derived Eshelby's equations in terms of tensorial multiplication. Zhao and Weng (1990) derived a 6 x 6 matrix marked S that represents the Eshelby solution for inclusion of either oblate geometry (penny shape) or prolate geometry (cigar shape) (Figure 6a,b). Let σi and σm be the stress vectors in the stiff inclusion and the soft matrix, respectively, and Li and Lm be the matrices of the Lamme' constants of the inclusion and matrix, respectively, then according to Benveniste (1987; Appendix A),

$$\sigma i = W\ \sigma m\ ,$$

where, W = Li T Lm-1 , T = [I + S Lm-1 (Li - Lm)] -1, and S is the matrix of Zhao and Weng (1990), I is the identity matrix, superscript -1 indicates inverse matrix, and matrix multiplication is assumed. Stress calculations were following Reches (1998).

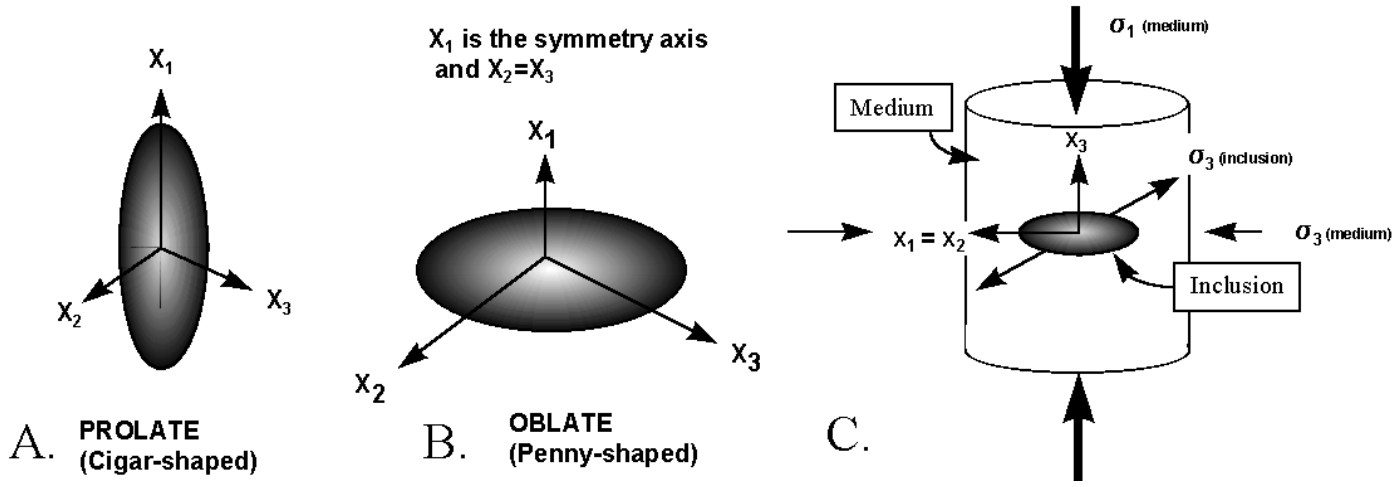

Figure 6: Notations for the 3D inclusion model.

Stress Amplifications in Inclusions

The stress amplification within a stiff inclusion is defined here by the ratio between a stress component in the inclusion and the corresponding stress component in the medium. According to this definition, tensile stress amplification and shear stress amplification are

$$A_{tensile} = (\sigma_3)_i / (\sigma_3)_m \text{ and,}$$

$$A_{shear} = (\sigma_1 - \sigma_3)_i / (\sigma_1 - \sigma_3)_m\ ,$$

where subscripts i and m denote stresses in the inclusion and medium, respectively. The solution to Eshelby's problem indicates that stress amplifications do not depend on absolute values of Young moduli, inclusion dimensions or stress intensities; rather, stress amplifications depend on the following ratios:

1. Stiffness ratio, K = (Young modulus of inclusion) / (Young modulus of medium),

2. Ratio of the principal axes of the inclusion: $X_1 : X_2 : X_3$,

3. Ratio of the principal stresses applied on the medium, $(\sigma_1)_m : (\sigma_2)_m : (\sigma_3)_m$.

Stress amplifications also depend on the Poisson ratios of the medium and the inclusion.

In one set of calculations, we determined the stress amplifications for axisymmetric penny-shape inclusions that are embedded in softer medium. The applied stresses on the medium are triaxial compressive, with principal stress axes $(\sigma_1)_m$, $(\sigma_2)_m$ and $(\sigma_3)_m$ paralleling to X_1, X_2 and X_3, respectively (Figure 6c). The stiffness ratio is constant, K = 5, and the Poisson ratio is 0.25 for the inclusion and 0.4 for the medium. The shape of the stiff inclusions ranges from spherical, $X_1 = X_2 = X_3 = 1$, to very thin layers, $X_1 = 0.0001$ and $X_2 = X_3 = 1$. The remote stress states range from almost uniaxial stress state, $(\sigma_1)_m = 1$ and $(\sigma_2)_m = (\sigma_3)_m = 0.1$, to

almost hydrostatic stress state, $(\sigma_1)_m = 1$, and $(\sigma_2)m = (\sigma_3)_m = 0.9$. The calculated amplifications of shear stress and tensile stress display few clear features for the selected parameters (Figure 7):

1. Stress amplification depends strongly on the stress state in the medium , $(\sigma_i)_m$. In general, stress states that are closer to hydrostatic generate less amplification then stress states which are closer to uniaxial.

2. For a given stress state, $(\sigma_i)_m$, stress amplification is almost constant for very flat inclusions with aspect ratios of $X_1 / X_2 < 0.01$.

3. For a given stress state, $(\sigma_i)_m$, stress amplification varies profoundly for inclusions with aspect ratios of $X_1 / X_2 > 0.1$.

4. Stress amplification is large for very flat inclusions. For example, for $(\sigma_3)_m < 0.5\ (\sigma_1)_m$ and $X_1 / X_2 < 0.01$, the least compressive stress in the inclusion, $(\sigma_3)_i$, is negative (true tensile) even when $(\sigma 3)_m$ are compressive. The absolute magnitude of $(\sigma_3)_i$ may be as high as 1.2 the magnitude of $(\sigma_3)_m$. Similar behavior is observed for the shear stress amplification.

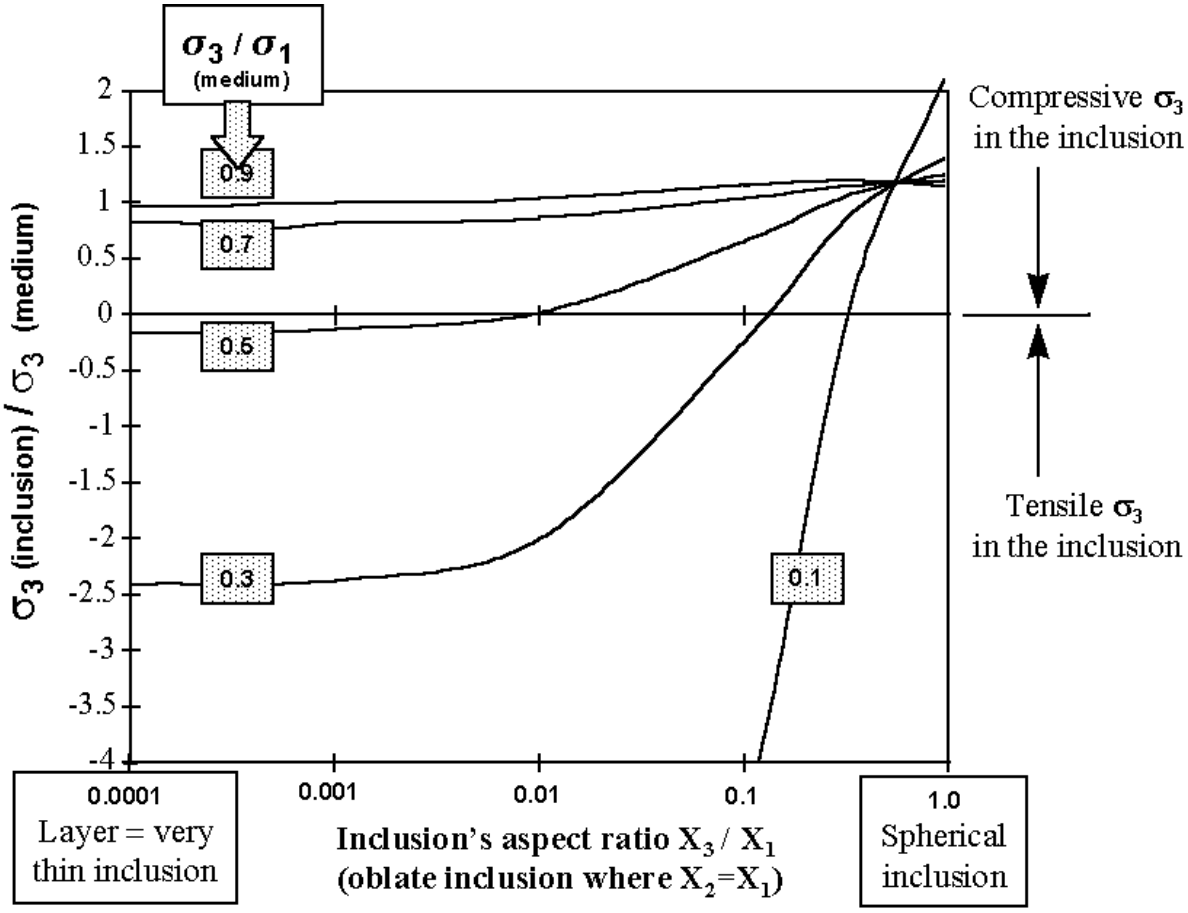

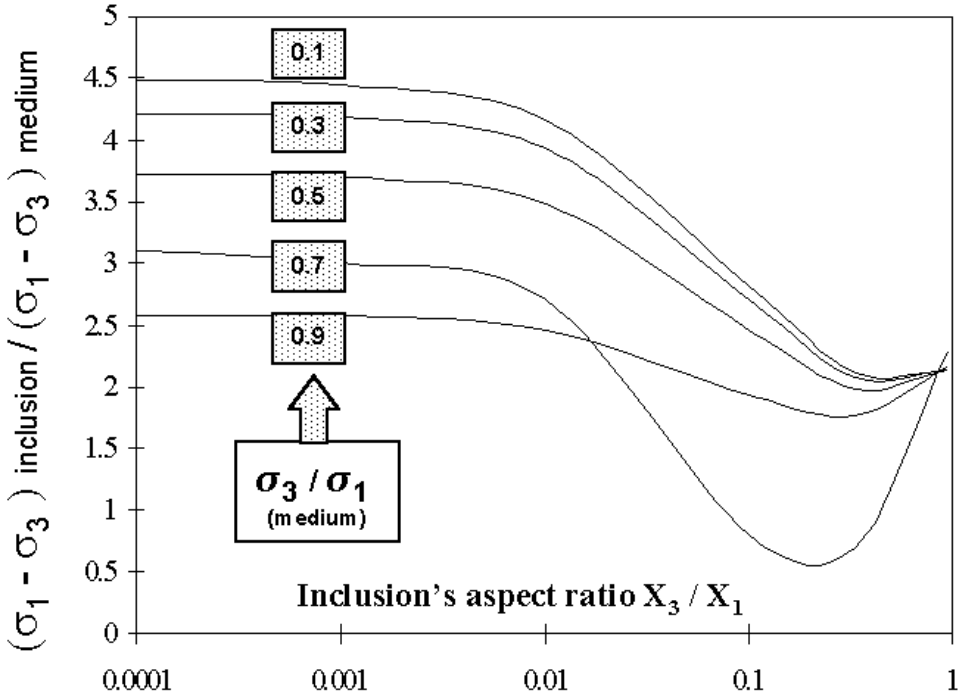

Figure 7: Stress amplification in stiff inclusions calculated for K= 5, $\nu_i = 0.25$ and $\nu_m = 0.4$.

A. (upper) Tensile stress amplification and B. (lower) shear stress amplification).

Applications to Layers

A typical rock layer is relatively thin with respect to its lateral extent, namely, L>>T in Figure 8. Such a layer may be idealized as an oblate ellipsoid with relative axes of X_1=1 and $X_2 = X_3 > > 100$. In a second set of calculations, stress amplification were derived for an ellipsoidal, flat layers of stiff limestone or dolomite that are embedded within a sequence of soft shales or marls (Figure 8). In the field, such sequences are usually subjected to combined loading of overburden load associated with the own weight of the rocks, and tectonic load associated with regional deformation. The overburden load generates vertical stress of

$$(\sigma_1)_m = \rho\, g\, h, \quad (1a)$$

and horizontal stresses that are equal to each other,

$$(\sigma_2)_m = (\sigma_3)_m = [\nu / (1 - \nu)]\, (\sigma_1)_m \quad (1b)$$

where ρ is the mean bulk density, g is earth gravity, and h is depth.

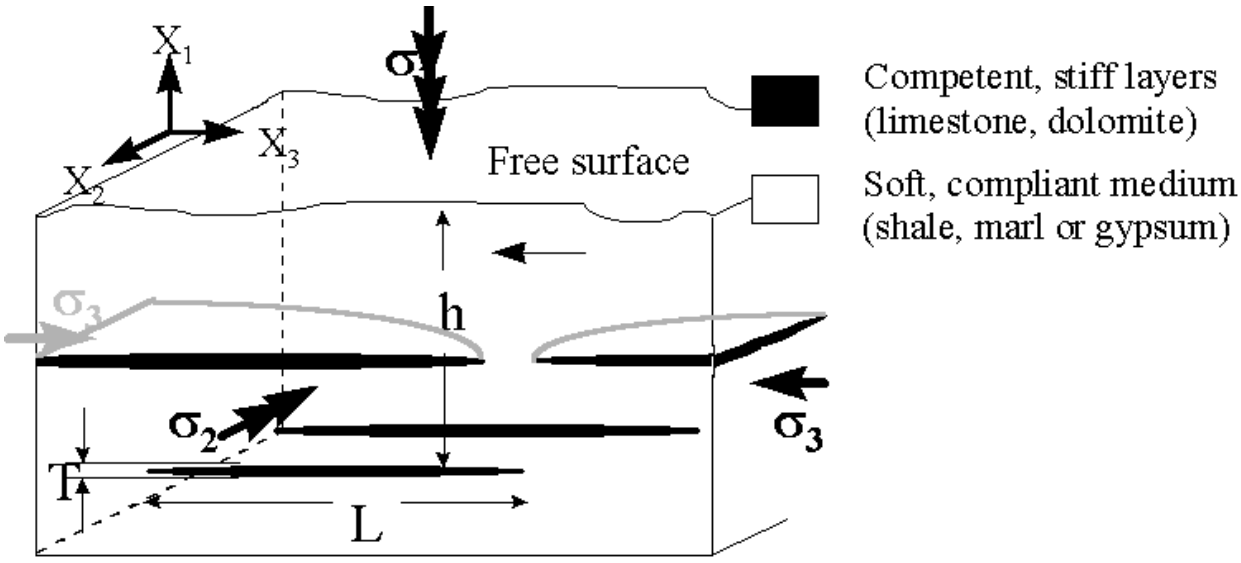

Figure 8: 3D view of the inclusion model for stiff layers embedded in soft rock sequence.

Krantz (1986) studied a system of normal faults developed in the Navajo Sandstone in Cedar Mountain area. It is likely that the studied Carmel Formation was subjected to the same tectonic extension as the underlying Navajo sandstone. Therefore, we examine here the tectonic loading of horizontal extension (normal faulting environment) that is superposed on the overburden load (Eqns. 1). Under such tectonic deformation, the vertical stress remains as above, and one of the horizontal stresses is reduced due to the tectonic extension. We chose a reduction of a factor of two following the arguments of Reches and Fink (1988). For a Poisson's ratio of $\nu = 0.3$ and the above selections, the vertical stress is

$$(\sigma_1)_m = \rho\, g\, h, \quad (2a)$$

the maximum horizontal stress is

$$(\sigma_2)_m = [\nu / (1 - \nu)]\, (\sigma_1)_m = 0.43\, \rho\, g\, h, \quad (2b)$$

and the least horizontal stress is

$$(\sigma_3)_m = 0.5\, (\sigma_2)_m = 0.21\, \rho\, g\, h. \quad (2c)$$

We used equations (1) and (2) to calculate the stress amplification in thin, oblate layers with aspect ratio of $X_1 / X_2 = 0.01$, and constant Poisson ratios of 0.25 and 0.30 for layer and medium. In these calculations, the stiffness ratio ranges from K = 1 to K= 10, and two stress states were considered: triaxial loading due to the overburden (Eqns. 1) and ploy axial loading due to combined overburden and tectonic loading (Eqns. 2). The results of these calculations are displayed by shear and tensile amplifications as a function of K (Figure 9); the stress magnitude in the host medium is normalized to unity. Figure 9b shows that the maximum shear stress in the layer $(\sigma_1 - \sigma_3)_i$ is 1.5 times the maximum shear stress in the medium $(\sigma_1 - \sigma_3)_m$ for K > 2., even without tectonic stresses. If tectonic stresses are active, $(\sigma_1 - \sigma_3)_i$ increases almost linearly with K. Similar behavior appears in Figure 9a for the tensile stresses. Here however, a more striking feature is shown: under tectonic loading, true tensile stresses develop within the layer for all cases of K > 1.5. This result implies that tensile fractures could develop within relatively stiff layers even when all applied loads are compressive.

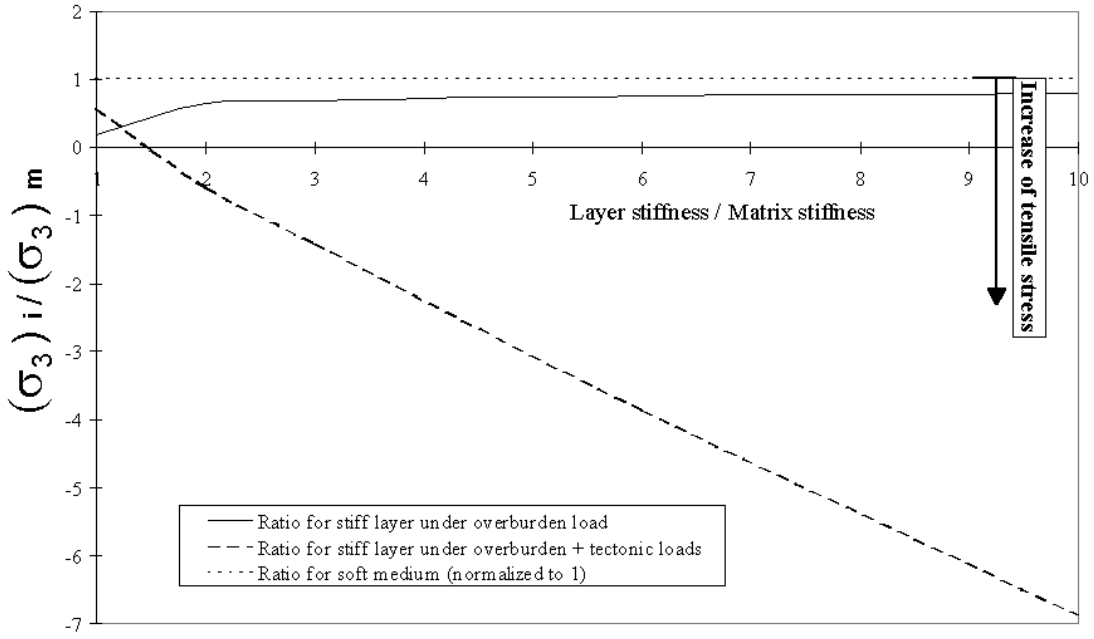

Figure 9: Amplification of maximum tensile stress within a stiff layer embedded in soft medium. $\nu_i = 0.25$ and $\nu_m = 0.3$. A. (above) Tensile stress amplification and B. (below) shear stress amplification.

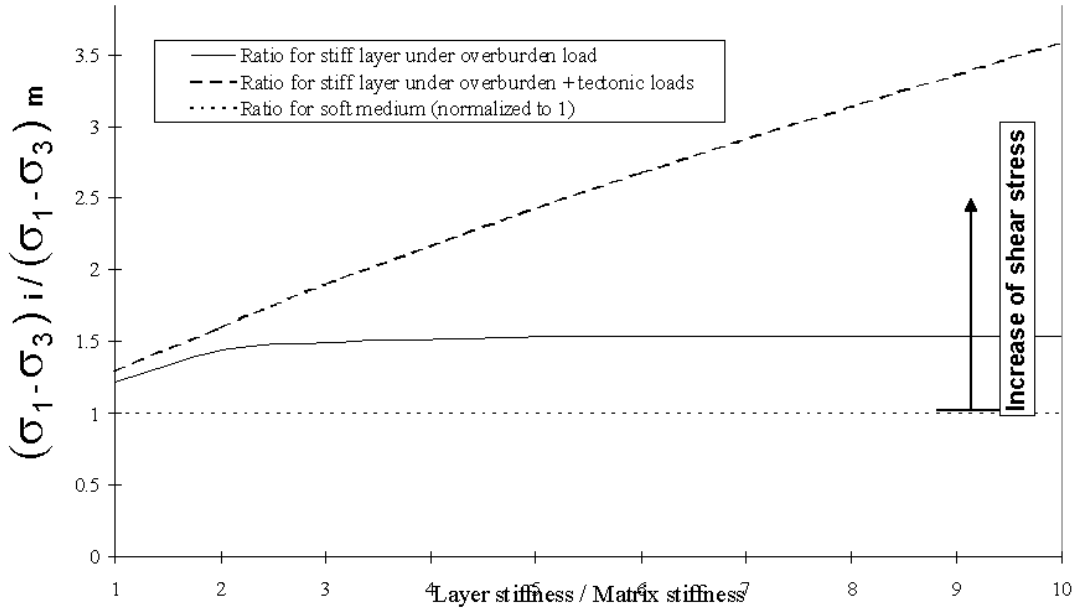

SUMMARY

We used Eshelby's model to calculate the expected stresses within thin, stiff layers embedded in a soft, layered sequence, under reasonable conditions of overburden loading and tectonic horizontal extension. The main results of Figures 7 and 9 are listed in Table 1. It is shown that tensile stresses should prevail in the layers even under compressive stress state in the medium. We envision that the limestone layers of Cedar Mountain area, fractured as follows. Under conditions of horizontal extension and vertical overburden stresses, the Carmel Formation was subjected to stress state that is close to the conditions of Eqn. (2). The overburden depth, h, at the time of fracturing is unknown but most likely it exceeded 1 km. By using bulk density of $\rho = 2{,}600$ kg/m^3 , and depth h = 1000 m, Eqns. (2) indicate stress state of $(\sigma_1)_m = 26$ MPa, $(\sigma_2)_m = 11$ MPa, and $(\sigma_3)_m = 5.5$ MPa. Assuming a reasonable stiffness ratio of K = 5, then Figure 9 indicate that the least stress in the inclusion is tensile, $(\sigma_3)_i = -3$ Mpa (or more tensile for greater depth). This high tensile stress could generate tensile fracturing even without the contribution of pore pressure (Weinberger et al., 1994). As the stiffness ratio depends on the lithology of the limestone layers, the amplified stresses would prevail as long as the tectonic stresses are active, leading to continuation of the fracturing and to the observed high fracture density.

TABLE 1: Summary of calculations (after Figures 7 and 9).

Aspect ratio of layer Remote stress state	Tensile stress amplification	Shear stress amplification			
$X_1/X_2 \leq 0.01$ (thin layer)	K =5	$\nu_i = 0.2$ $\nu_m = 0.4$	$(\sigma_2)m=(\sigma_3)_m \leq 0.5(\sigma_1)_m$ (compressive)	true tension in the stiff layer	3.5-4.5 larger than remote
$X_1/X_2 \leq 0.01$	$K \geq 1.5$	$\nu_i = 0.2$ $\nu_m = 0.3$	$(\sigma_2)m=(\sigma_3)_m = 0.43(\sigma_1)_m$ (overburden)	no true tension in the stiff layer	$\approx$ 1.5 larger than remote
$X_1/X_2 \leq 0.01$	$K \geq 1.5$	$\nu_i = 0.2$ $\nu_m = 0.3$	$(\sigma_2)m= 0.43(\sigma_1)_m$ $(\sigma_3)_m = 0.21(\sigma_1)_m$ (overburden + tectonic)	true tension in layer (for K=10, $(\sigma_3)_i = - 6.5\ (\sigma_3)_m$	for K=10, 3.5 larger than remote

ACKNOWLEDGMENT

Many thanks to Martin Pruatt for field assistance, to Amir Eidelman and Amir Sagy for useful discussions, and to Rod Holocombe for his stereoplot program. Partial support was provided by the Rock Mechanics Consortium, Oklahoma Univ., Norman (report RMC-93-21), and by Yisum Fund, Hebrew Univ., Jerusalem.

References

Benveniste, Y., A new approach to the application of Mori-Tanaka theory in composite materials, *Mech. Materials,* 1987, 6, 147-157.

Eidelman, A., and Reches, Z., Fractured pebbles-A new stress indicator, *Geology*, 1992, 20, 301-304.

Eidelman, A., (1994). *Faulting and fracturing in the Arava, Israel: the structure of a short strike-slip fault and the development of tensile fractures in pebbles,* Ph. D., dissertation, Hebrew Univ., 137 p. (in Hebrew with abstract in English).

Eshelby, J. D., The determination of the elastic field of an ellipsoidal inclusion, and related problems. *Proc. Roy. Soc.,* 1957, 252, 376-395.

Harris, J.F., Taylor, G. L. and Walper, J.L., Relation of deformational fractures in sedimentary rocks to regional and local structure [Wyoming]. *Bull. Am. Assoc. Petrol. Geol.,* 1960, 44, 1853-1873.

Hodgson, R.A., Classification of structures on joint surfaces. *American J Science.,* 1961, 259, 493-502.

Gross, M. R., The origin and spacing of cross joints; examples from the Monterey Formation, Santa Barbara coastline, California, *J. Structural Geol.,* 1993, 15, 737-751.

Jaeger, J. C. and Cook, N. G. W., (1979). *Fundamentals of Rock Mechanics*, Champan and Hall, 593 pp.

Krantz, R. W., Multiple fault sets and three-dimensional strain; theory and application, *J. Structural Geol.,* 1988, 10, 225-237.

Lorenz, J.C., Teufel, L.W., and Warpinski, N. R., Regional fractures I: A mechanism for the formation of regional fractures at depth in flat-lying reservoirs, *Bull. Am. Assoc. Petrol. Geol.,* 1991, 75, 1714-1737.

Mura, T., (1987). *Micromechanics of defects in solids,* 2nd ed. Martinus Nijhoff, Dordrecht.

Nelson, R. A., (1985). *Geological Analysis of Naturally Fractured Reservoirs,* Gulf Publication Co., 320 pp.

Price N. J. and J. W. Cosgrove, (1990). *Analysis of geological structures,* Cambridge, 502 p.

Reches, Z., (1972). *Jointing in the Hazera and Hathira monoclines, northern Negev,* M.Sc. thesis, Hebrew University, Jerusalem, (in Hebrew with Abstract in English).

Reches, Z., and J. Fink, The mechanism of the emplacement of the Inyo Dike, Long Valley, California, *J. Geophysical Res.,* 1988, 93, 4321-4335.

Reches, Z., (1998). *SoftStructure-Structural Geology on a Personal Computer, programs for quantitative analysis in Structural Geology,* web site: http://earth.es.huji.ac.il/reches/

Weinberger R., Reches Z., Scott T.E., and Eidelman A., Tensile strength of rocks in four-point beam tests, in Nelson P. and Laubach (eds), Rock mechanics models and measurements challenges for industry, *Proc. 1st North Am. Rock Mechanics Symp., Austin,* Balkema, Rotterdam, 1994, p. 435-442.

Zhao, Y.H. and Weng, G.J, Theory of plasticity for a class of inclusion and fiber-reinforced composites, in Weng et al. (eds), *Micromechanics and inhomogeneity,* Springer-Verlag, 1990, p. 599-622.